

Hidden elastic softness of low-symmetry frustrated ATi_2O_5 ($A = \text{Co, Fe}$)

Tadataka Watanabe^{1,*}, Kazuya Takayanagi¹, Ray Nishimura¹, Yoshiaki Hara²,
Dharmalingam Prabhakaran³, Roger D. Johnson⁴, and Stephen J. Blundell³

¹*Department of Physics, College of Science and Technology,
Nihon University, Chiyoda, Tokyo 101-8308, Japan*

²*National Institute of Technology, Ibaraki College, Hitachinaka 312-8508, Japan*

³*Department of Physics, Clarendon Laboratory, Oxford University,
Parks Road, Oxford OX1 3PU, United Kingdom and*

⁴*Department of Physics and Astronomy and London Centre for Nanotechnology,
University College London, London WC1E 6BT, United Kingdom*

(Dated: August 8, 2024)

Orthorhombic pseudobrookites CoTi_2O_5 and FeTi_2O_5 have a low-symmetry crystal structure comprising magnetic $\text{Co}^{2+}/\text{Fe}^{2+}$ ions and nonmagnetic Ti^{4+} ions, where the orbital-nondegenerate $\text{Co}^{2+}/\text{Fe}^{2+}$ ions form one-dimensional chains running along the orthorhombic a axis. These compounds undergo an antiferromagnetic phase transition at $T_N \sim 26$ K for CoTi_2O_5 and $T_N \sim 40$ K for FeTi_2O_5 . We perform ultrasound velocity measurements on single crystals of CoTi_2O_5 and FeTi_2O_5 . The measurements of these compounds reveal that the symmetry-lowering elastic modes of shear elastic moduli exhibit unusual elastic softness in the paramagnetic phase above T_N . This elastic softness indicates the presence of spin-lattice-coupled fluctuations above T_N that should be a precursor to the symmetry-lowering lattice distortion at T_N . Furthermore, it is revealed that the magnitude of the unusual elastic softness is larger in CoTi_2O_5 than in FeTi_2O_5 , which indicates that the spin-lattice coupling is stronger in CoTi_2O_5 than in FeTi_2O_5 . The present study suggests that CoTi_2O_5 and FeTi_2O_5 are unique spin Jahn–Teller systems with low crystal symmetry, where, although the nature of exchange interactions is quasi-one-dimensional, the three-dimensional spin-lattice coupling releases the frustration by further lowering the crystal symmetry.

I. INTRODUCTION

Frustrated magnets provide fertile ground for exploring novel correlated phenomena emerging from competing magnetic interactions [1]. In a frustrated system with spin-lattice coupling, the spin degeneracy can be lifted by symmetry-lowering lattice distortion [2,3]. This effect is called the spin Jahn–Teller (spin-JT) effect because its mechanism is analogous to the Jahn–Teller effect in orbital-degenerate systems where the spontaneous lattice distortion reduces the crystal symmetry to lift the orbital degeneracy [4]. The spin-JT effect was initially proposed for cubic pyrochlore antiferromagnets where spins form a lattice of corner-sharing tetrahedra [2,3]. For real pyrochlore antiferromagnets, the spin-JT mechanism has been applied to explain the magnetostructural transitions of some cubic spinels, where a cubic-to-tetragonal lattice distortion releases the frustration [5–7].

Recently, orthorhombic pseudobrookites ATi_2O_5 ($A = \text{Co, Fe}$), having much lower symmetry than the prototypical spin-JT system of cubic spinels, have been proposed as candidate spin-JT systems [8,9]. These pseudobrookites comprise magnetic Co^{2+} ($3d^7$, $S = 3/2$) or Fe^{2+} ($3d^6$, $S = 2$) ions and nonmagnetic Ti^{4+} ions. In addition, the magnetic A^{2+} ions occupying the equivalent crystal sites form one-dimensional (1D) chains running along the orthorhombic a axis [Fig. 1]. In ATi_2O_5 , the magnetic A^{2+} ions with C_{2v} site symmetry have no orbital degeneracy, and the interchain exchange interactions are considered to be frustrated [8,9].

ATi_2O_5 undergoes an antiferromagnetic (AF) transi-

tion at $T_N \sim 26$ K for CoTi_2O_5 and $T_N \sim 40$ K for FeTi_2O_5 [8–10,12]. For CoTi_2O_5 , the long-range AF order with the propagation vector $\mathbf{q} = (\pm\frac{1}{2}, \frac{1}{2}, 0)$ has been identified in neutron powder diffraction and muon-spin rotation experiments [8]. The emergence of this AF order requires a symmetry-lowering lattice distortion for the orthorhombic CoTi_2O_5 . Thus, this orbital-nondegenerate frustrated antiferromagnet is suggested to be a spin-JT magnet. For FeTi_2O_5 , by combining muon spin rotation and x-ray diffraction experiments with density functional theory calculations, it has been demonstrated that the crystal and AF structures are the same as those of CoTi_2O_5 [9]. This suggests that not only CoTi_2O_5 but also FeTi_2O_5 are spin-JT magnets. Although the symmetry-lowering lattice distortion in the AF state has not yet been experimentally resolved in either CoTi_2O_5 or FeTi_2O_5 , recent resonant elastic x-ray scattering experiments in CoTi_2O_5 and thermal expansion and magnetostriction measurements in FeTi_2O_5 revealed the presence of magnetoelastic coupling, which supports the spin-JT scenario in ATi_2O_5 [11,12].

In this paper, we present ultrasound velocity measurements of the low-symmetry orthorhombic ATi_2O_5 ($A = \text{Co, Fe}$), from which we determine the elastic moduli of these compounds. The sound velocity or elastic modulus is a useful probe with which to extract symmetry-resolved thermodynamic information from a crystal [13]. Furthermore, as the ultrasound velocity can be measured with a high precision of approximately parts per million, its measurements can sensitively probe elastic anomalies driven by phase transitions, fluctuations, and excitations [13]. In magnets, the modified sound dispersions caused

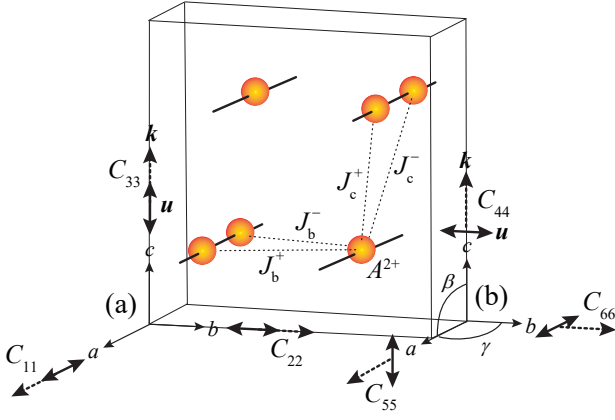


FIG. 1: (Color online) Magnetic A^{2+} sites of ATi_2O_5 ($A = \text{Co, Fe}$) in the orthorhombic crystal unit cell, which form 1D a -axis chains (solid lines). The dotted lines indicate the interchain neighboring exchange interactions J_b^\pm and J_c^\pm . With the crystal axes (a) and (b), the propagation vector \mathbf{k} and polarization vector \mathbf{u} of the sound waves for (a) compressive elastic moduli C_{11} , C_{22} , and C_{33} , and (b) shear elastic moduli C_{44} , C_{55} , and C_{66} are indicated. The angles β and γ between the crystal axes (b) correspond to the shear angles that are respectively tilted by the sound waves for C_{55} ($\mathbf{k} \parallel \mathbf{a}$, $\mathbf{u} \parallel \mathbf{c}$) and C_{66} ($\mathbf{k} \parallel \mathbf{b}$, $\mathbf{u} \parallel \mathbf{a}$).

by magnetoelastic coupling allow the extraction of detailed information on the interplay of the lattice, spin, and orbital degrees of freedom [13–32].

In the spin-JT system, spin-lattice coupling induces a structural transition that lowers the crystal symmetry. For instance, the representative spin-JT system of chromite spinel ACr_2O_4 ($A = \text{Mg, Zn}$) has an AF transition at $T_N \sim 13$ K coinciding with the cubic-to-tetragonal lattice distortion [5, 6]. For ACr_2O_4 , the ultrasound velocity measurements in the single crystal revealed that the temperature (T) dependence of the tetragonal shear modulus $(C_{11} - C_{12})/2$ exhibits Curie-type ($\sim -1/T$ -type) softening upon cooling in the cubic paramagnetic phase ($T > T_N$), which is a precursor to the cubic-to-tetragonal lattice distortion at T_N [14]. This elastic anomaly above T_N indicates the presence of spin-lattice-coupled fluctuations in the paramagnetic phase of ACr_2O_4 , which is referred to as the dynamical spin-JT effect. In the present study of the orthorhombic pseudobrookites CoTi_2O_5 and FeTi_2O_5 , we find the presence of unusual elastic softness in the paramagnetic phase above T_N , which suggests that the dynamical spin-JT effect emerges even in low-symmetry frustrated magnets.

II. EXPERIMENTAL

Single crystals of CoTi_2O_5 with $T_N \sim 26$ K and FeTi_2O_5 with $T_N \sim 40$ K were grown adopting the floating-zone method [8, 9]. The ultrasound velocities were measured adopting the phase-comparison technique

TABLE I: Elastic moduli for ATi_2O_5 ($A = \text{Co, Fe}$) with an orthorhombic crystal structure, and the corresponding sound mode (propagation vector \mathbf{k} and polarization vector \mathbf{u}) and irreducible representation (irrep).

Elastic modulus	Sound mode (\mathbf{k} and \mathbf{u})	Irrep
C_{11}	Longitudinal wave ($\mathbf{k} \parallel \mathbf{u} \parallel \mathbf{a}$)	A_g
C_{22}	Longitudinal wave ($\mathbf{k} \parallel \mathbf{u} \parallel \mathbf{b}$)	A_g
C_{33}	Longitudinal wave ($\mathbf{k} \parallel \mathbf{u} \parallel \mathbf{c}$)	A_g
C_{44}	Transverse wave ($\mathbf{k} \parallel \mathbf{c}$, $\mathbf{u} \parallel \mathbf{b}$)	B_{3g}
C_{55}	Transverse wave ($\mathbf{k} \parallel \mathbf{a}$, $\mathbf{u} \parallel \mathbf{c}$)	B_{2g}
C_{66}	Transverse wave ($\mathbf{k} \parallel \mathbf{b}$, $\mathbf{u} \parallel \mathbf{a}$)	B_{1g}

with longitudinal and transverse sound waves at a frequency of 30 MHz, where the ultrasound velocity or elastic modulus can be measured with a high precision of approximately parts per million. The ultrasound waves were generated and detected by LiNbO_3 transducers glued to parallel mirror surfaces of the crystal, which were perpendicular to the a , b , and c orthorhombic axes. Measurements were taken to determine the symmetrically independent elastic moduli of the orthorhombic crystal, specifically the compressive elastic moduli C_{11} , C_{22} , and C_{33} and the shear elastic moduli C_{44} , C_{55} , and C_{66} (see Table I). In Fig. 1, the propagation vector \mathbf{k} and polarization vector \mathbf{u} of the sound waves for the respective elastic moduli are indicated along with the magnetic A^{2+} sites of ATi_2O_5 ($A = \text{Co, Fe}$) in the orthorhombic crystal unit cell, which form the 1D a -axis chains. As indicated in Fig. 1(a), the longitudinal sound wave corresponding to the compressive elastic modulus C_{11} propagates along the magnetic A^{2+} chains ($\mathbf{k} \parallel \mathbf{a}$), whereas the longitudinal waves corresponding to the compressive moduli C_{22} and C_{33} propagate orthogonal to the A^{2+} chains ($\mathbf{k} \perp \mathbf{a}$). Likewise, in Fig. 1(b), the transverse sound wave corresponding to the shear elastic modulus C_{55} propagates along the A^{2+} chains ($\mathbf{k} \parallel \mathbf{a}$), whereas the transverse waves corresponding to the shear C_{44} and C_{66} propagate orthogonal to the A^{2+} chains ($\mathbf{k} \perp \mathbf{a}$). The sound velocities of CoTi_2O_5 (FeTi_2O_5) measured at a room temperature of 300 K are 8820 m/s (8600 m/s) for C_{11} , 8750 m/s (6380 m/s) for C_{22} , 8630 m/s (7620 m/s) for C_{33} , 3920 m/s (3600 m/s) for C_{44} , 4300 m/s (4090 m/s) for C_{55} , and 4040 m/s (3660 m/s) for C_{66} .

III. RESULTS AND DISCUSSION

A. CoTi_2O_5

Figure 2(a)–(c) respectively present the temperature (T) dependence of the compressive elastic moduli $C_{11}(T)$, $C_{22}(T)$, and $C_{33}(T)$ in CoTi_2O_5 . $C_{11}(T)$ [Fig. 2(a)] and $C_{33}(T)$ [Fig. 2(c)] exhibit monotonic hardening upon cooling from 300 to 2 K, as is usually observed in solids [33]. In addition, $C_{22}(T)$ [Fig. 2(b)] exhibits ordinary monotonic hardening upon cooling from 300 to $T_N \sim 26$

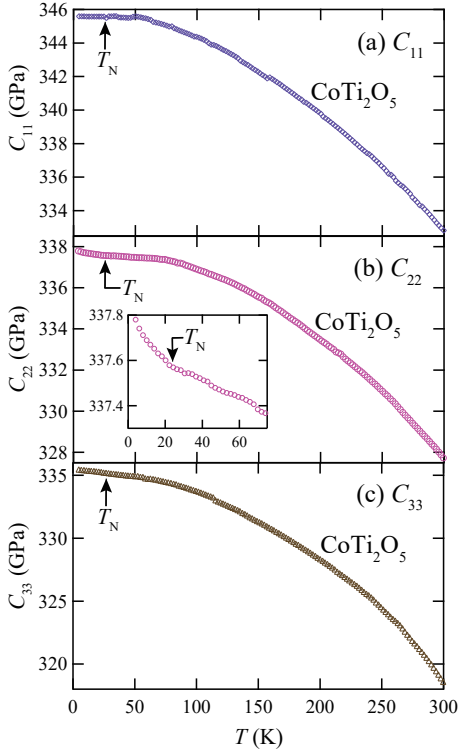


FIG. 2: (Color online) (a)–(c) Compressive elastic moduli of CoTi_2O_5 as functions of T : (a) $C_{11}(T)$, (b) $C_{22}(T)$, and (c) $C_{33}(T)$. The inset in (b) shows the expanded view of $C_{22}(T)$ below 75 K. The labeled arrows indicate $T_N \sim 26$ K of CoTi_2O_5 .

K and a small slope change of hardening at $T_N \sim 26$ K.

Figure 3(a)–(c) respectively depict the T dependence of the shear elastic moduli $C_{44}(T)$, $C_{55}(T)$, and $C_{66}(T)$ in CoTi_2O_5 . In these plots, all the elastic moduli exhibit hardening upon cooling from 300 to ~ 50 K, but below ~ 50 K, only $C_{55}(T)$ [Fig. 3(b)] exhibits Curie-type ($\sim -1/T$ -type) softening upon cooling to $T_N \sim 26$ K. Furthermore, $C_{55}(T)$ [Fig. 3(b)] and $C_{66}(T)$ [Fig. 3(c)] exhibit a discontinuous anomaly at $T_N \sim 26$ K, whereas there is no anomaly in $C_{44}(T)$ [Fig. 3(a)].

For CoTi_2O_5 , considering the absence of orbital degeneracy at the Co^{2+} site, the observed elastic anomalies in $C_{\Gamma}(T)$, namely the Curie-type softening above T_N in $C_{55}(T)$ [Fig. 3(b)] and the discontinuous anomalies at T_N in $C_{22}(T)$ [Fig. 2(b)], $C_{55}(T)$ [Fig. 3(b)] and $C_{66}(T)$ [Fig. 3(c)] should have magnetic origins where the spin degrees of freedom play significant roles. Such elastic anomalies are attributed to magnetoelastic coupling acting on the exchange interactions, where the exchange striction arises from a modulation of the exchange interactions by ultrasound as follows: ^[13]

$$H_{\text{exs}} = \sum_{ij} [J(\delta + \mathbf{u}_i - \mathbf{u}_j) - J(\delta)] \mathbf{S}_i \cdot \mathbf{S}_j. \quad (1)$$

Here, $\delta = \mathbf{R}_i - \mathbf{R}_j$ is the distance between two mag-

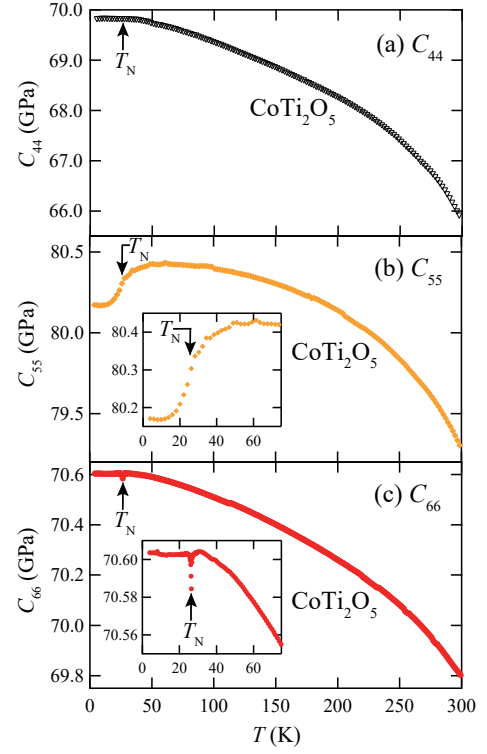


FIG. 3: (Color online) (a)–(c) Shear elastic moduli of CoTi_2O_5 as functions of T : (a) $C_{44}(T)$, (b) $C_{55}(T)$, and (c) $C_{66}(T)$. The insets in (b) and (c) are respectively the expanded views of $C_{55}(T)$ and $C_{66}(T)$ below 75 K. The labeled arrows indicate $T_N \sim 26$ K of CoTi_2O_5 .

netic ions, and \mathbf{u}_i is the displacement vector for the ion with equilibrium position \mathbf{R}_i . When a sound wave with polarization \mathbf{u} and propagation \mathbf{k} is given by $\mathbf{u} = \mathbf{u}_0 \exp[i(\mathbf{k} \cdot \mathbf{r} - \omega t)]$, where \mathbf{u}_0 and ω are the respective amplitude and frequency, the exchange striction of Eq. (1) is rewritten as ^[34]

$$H_{\text{exs}} = \sum_i \left(\frac{\partial J}{\partial \delta} \cdot \mathbf{u}_0 \right) (\mathbf{k} \cdot \delta) (\mathbf{S}_i \cdot \mathbf{S}_{i+\delta}) e^{i(\mathbf{k} \cdot \mathbf{R}_i - \omega t)}. \quad (2)$$

Here, the exponential is expanded to first order because with a 30-MHz ultrasound frequency $k\delta \ll 1$. Eq. (2) indicates that both the longitudinal and transverse sound waves can couple to the spin system via the exchange striction mechanism, depending on the directions of polarization \mathbf{u} and propagation \mathbf{k} relative to the exchange path δ .

For CoTi_2O_5 with 1D Co^{2+} chains, one possible origin for the observed elastic anomalies is the spin-Peierls effect, where the lattice distortion along the spin chain direction occurs at the transition temperature T_{sp} . In the T dependence of the elastic moduli of the spin-Peierls system, it is expected from the exchange striction mechanism [Eq. (2)] that only the compressive modulus along the spin chain direction has a pronounced

anomaly at T_{sp} , and the shear moduli have no anomaly, as observed for the prototypical spin-Peierls compound CuGeO_3 [30–32]. Thus, for CoTi_2O_5 , although a quasi-1D magnetic character has been experimentally suggested [10], the absence of an elastic anomaly at T_N in the spin-chain-direction (a -axis) compressive modulus $C_{11}(T)$ [Fig. 2(a)] rules out a possible spin-Peierls transition at T_N . In addition, Curie-type softening in the shear modulus $C_{55}(T)$ above T_N [Fig. 3(b)] should have an origin other than the spin-Peierls instability.

In magnets, Curie-type softening in the T dependence of the elastic modulus $C_\Gamma(T)$ emerges as a precursor to a structural transition, which is driven by the coupling of the lattice to the electronic degrees of freedom [13,14,18,19,22–29]. Thus, the Curie-type softening in the symmetry-lowering elastic mode $C_{55}(T)$ of CoTi_2O_5 above T_N should be a precursor to the symmetry-lowering lattice distortion at T_N . Such a precursor softening to the structural transition is well known to occur as a result of the Jahn–Teller effect in orbital-degenerate systems [13]. However, the absence of orbital degeneracy at the Co^{2+} site in CoTi_2O_5 rules out such orbital effects. Thus, the Curie-type softening in $C_{55}(T)$ of CoTi_2O_5 is most probably due to the spin-JT effect [2,3]. It is noted that the magnitude of the Curie-type softening in CoTi_2O_5 ($\Delta C_{55}/C_{55} \sim 0.15\%$) [Fig. 3(b)] is much smaller than that in the prototypical spin-JT system of chromite spinel ACr_2O_4 ($\Delta C_\Gamma/C_\Gamma \sim 50\%$) [14]. This indicates that the magnitude of Curie-type softening in a low-symmetry spin-JT system like orthorhombic CoTi_2O_5 is smaller than that in a high-symmetry spin-JT system like cubic ACr_2O_4 . For CoTi_2O_5 , the small magnitude of the Curie-type softening above T_N is compatible with the magnitude of the lattice distortion below T_N being too small to have been resolved experimentally [8].

In the spin-JT system, the T dependence of the elastic modulus $C_\Gamma(T)$ in the paramagnetic phase can be decomposed into the “usual” background component $C_\Gamma^{(0)}(T)$ and “unusual” spin-JT component $\delta C_\Gamma^{sJT}(T)$: $C_\Gamma(T) = C_\Gamma^{(0)}(T) + \delta C_\Gamma^{sJT}(T)$, where $C_\Gamma^{(0)}(T)$ exhibits monotonic hardening with decreasing T [33], and $\delta C_\Gamma^{sJT}(T)$ contributes to the Curie-type softening expressed by $\delta C_\Gamma^{sJT}(T) \sim -1/T$ [14]. For the prototypical spin-JT system ACr_2O_4 , the observation of the huge Curie-type softening in $C_\Gamma(T)$ ($\Delta C_\Gamma/C_\Gamma \sim 50\%$) indicates that the contribution of $\delta C_\Gamma^{sJT}(T)$ is much larger than the hardening magnitude of $C_\Gamma^{(0)}(T)$, where $C_\Gamma^{(0)}(T)$ can be assumed to be T independent [14]. For the low-symmetry spin-JT system CoTi_2O_5 , the observation of the small Curie-type softening in $C_{55}(T)$ ($\Delta C_{55}/C_{55} \sim 0.15\%$) [Fig. 3(b)] indicates that the contribution of $\delta C_\Gamma^{sJT}(T)$ is small, comparable to that of $C_\Gamma^{(0)}(T)$. Thus, for CoTi_2O_5 , although the small Curie-type softening is observed only in $C_{55}(T)$ [Figs. 2 and 3], we should verify the presence of “hidden” elastic softness arising from the spin-JT component $\delta C_\Gamma^{sJT}(T)$ in $C_\Gamma(T)$ other than $C_{55}(T)$.

For the elastic modulus $C_\Gamma(T)$ of CoTi_2O_5 exhibiting hardening upon cooling, the contribution of the “hidden” spin-JT component $\delta C_\Gamma^{sJT}(T)$ should depend on the elastic mode; i.e., a larger contribution of the spin-JT component $\delta C_\Gamma^{sJT}(T)$ corresponds to a smaller magnitude of the observed hardening of $C_\Gamma(T)$. We here compare the hardening magnitudes in $C_\Gamma(T)$ of CoTi_2O_5 [Figs. 2 and 3]. Figure 4 depicts the relative shifts of compressive $C_{11}(T)$, $C_{22}(T)$, and $C_{33}(T)$ of CoTi_2O_5 [Fig. 4(a), from Fig. 2] and shear $C_{44}(T)$, $C_{55}(T)$, and $C_{66}(T)$ of CoTi_2O_5 [Fig. 4(b), from Fig. 3]. It is clearly seen that the hardening magnitudes of not only $C_{55}(T)$ but also $C_{66}(T)$ [Fig. 4(b)] are smaller than those of other elastic moduli, indicating the large contribution of the spin-JT component $\delta C_\Gamma^{sJT}(T)$ in not only $C_{55}(T)$ but also $C_{66}(T)$. The inset in Fig. 4(b) illustrates the relative shift of the experimental $C_{66}(T)$ and its decomposed components of the background component $C_{66}^{(0)}(T)$ and spin-JT component $\delta C_{66}^{sJT}(T)$, where $C_{66}(T) = C_{66}^{(0)}(T) + \delta C_{66}^{sJT}(T)$. As illustrated in this figure, the hardening magnitude of the experimental $C_{66}(T)$ should be suppressed relative to the background component $C_{66}^{(0)}(T)$ owing to the presence of the spin-JT component $\delta C_{66}^{sJT}(T)$. Similarly to $C_{66}(T)$ [inset in Fig. 4(b)], the experimental $C_{55}(T)$ [Fig. 4(b)] should comprise the background component $C_{55}^{(0)}(T)$ and “hidden” spin-JT component $\delta C_{55}^{sJT}(T)$, where $\delta C_{55}^{sJT}(T)$ “shows up” in the experimental $C_{55}(T)$ at $T_N < T \lesssim 50$ K [Figs. 3(b) and 4(b)]. For CoTi_2O_5 , the precursor to the spin-JT transition above T_N should be characterized as the “hidden” softening in $C_{55}(T)$ and $C_{66}(T)$.

For CoTi_2O_5 , considering that the strain generated by ultrasound in $C_{55}(\mathbf{k} \parallel \mathbf{a}, \mathbf{u} \parallel \mathbf{c})$ tilts the angle β between the a and c crystal axes [Fig. 1(b) and inset in Fig. 4(c)], Curie-type softening in $C_{55}(T)$ above T_N [Fig. 3(b)] should be a precursor to the ac -plane shear lattice distortion at T_N . This β -tilt lattice distortion at T_N releases the frustration of the c -axis-stacking interchain exchange interactions J_c^\pm [Fig. 1 and inset in Fig. 4(c)]. In addition, considering that the strain generated by ultrasound in $C_{66}(\mathbf{k} \parallel \mathbf{b}, \mathbf{u} \parallel \mathbf{a})$ tilts the angle γ between the a and b crystal axes [Fig. 1(b) and inset in Fig. 4(d)], the “hidden” Curie-type softening in $C_{66}(T)$ above T_N [Fig. 4(b)] should be a precursor to the ab -plane shear lattice distortion at T_N . This γ -tilt lattice distortion at T_N releases the frustration of the b -axis-stacking interchain exchange interactions J_b^\pm [Fig. 1 and inset in Fig. 4(d)]. Thus, for CoTi_2O_5 , the Curie-type softening in $C_{55}(T)$ and $C_{66}(T)$ above T_N should be a precursor to the orthorhombic-to-triclinic lattice distortion at T_N , which tilts the angles β and γ [Fig. 1(b)]. This suggests that, for CoTi_2O_5 , the interchain frustrations of J_b^\pm and J_c^\pm [Fig. 1] are simultaneously released at T_N through spin-lattice coupling, resulting in the formation of AF order with the propagation vector $\mathbf{q} = (\pm\frac{1}{2}, \frac{1}{2}, 0)$ [8].

In the spin-JT system, the T dependence of the elastic modulus $C_\Gamma(T)$ is explained by assuming a coupling of ul-

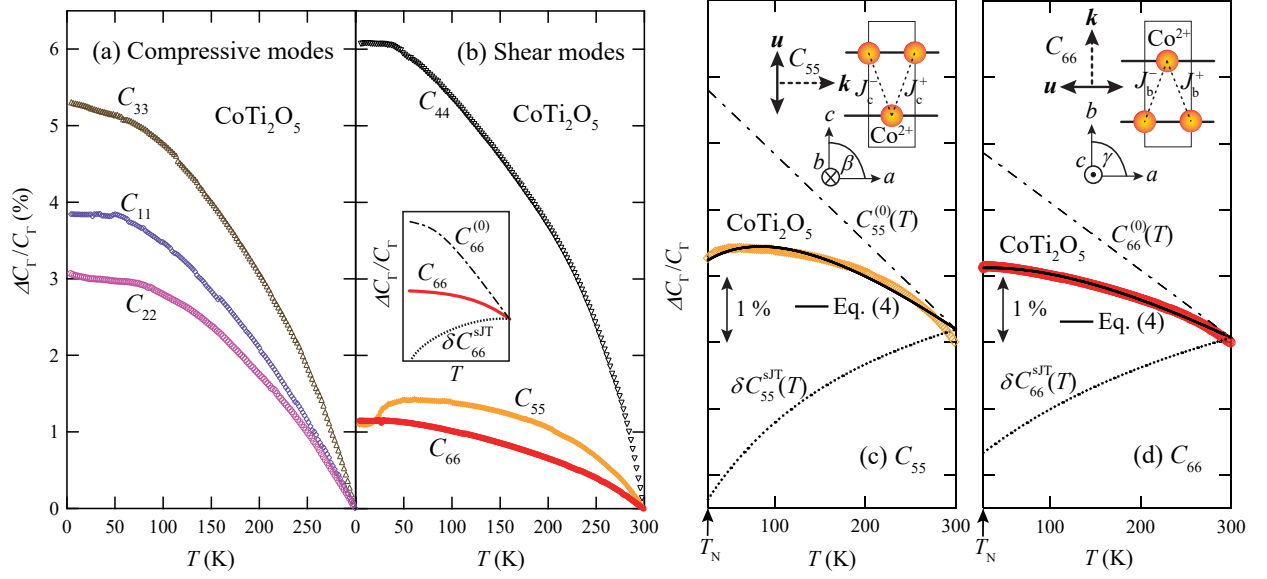


FIG. 4: (Color online) (a) and (b) Comparison of the relative shifts of the elastic moduli $C_r(T)$ of CoTi_2O_5 : (a) compressive $C_{11}(T)$, $C_{22}(T)$, and $C_{33}(T)$ and (b) shear $C_{44}(T)$, $C_{55}(T)$, and $C_{66}(T)$. The experimental data in (a) and (b), respectively, are identical to those in Figs. 2 and 3. The inset in (b) illustrates the relative shift of $C_{66}(T)$ and its decomposed components of the “usual” background component $C_{66}^{(0)}(T)$ and “unusual” spin-JT component $\delta C_{66}^{sJT}(T)$, where $C_{66}(T) = C_{66}^{(0)}(T) + \delta C_{66}^{sJT}(T)$. (c) Relative shift of $C_{55}(T)$ of CoTi_2O_5 at $T > T_N$ [squares, from (b)]. (d) Relative shift of $C_{66}(T)$ of CoTi_2O_5 at $T > T_N$ [circles, from (b)]. The solid curves in (c) and (d) are fittings of Eq. (4) to the experimental $C_r(T)$. The dashed-dotted curves in (c) and (d) are the background components $C_r^{(0)}(T)$ in the fittings of Eq. (4). The dotted curves in (c) and (d) are the spin-JT components $\delta C_r^{sJT}(T)$ in the fittings of Eq. (4). The insets in (c) and (d) respectively illustrate the ac -plane and ab -plane projections of the unit cell shown in Fig. 1 along with the sound propagation vector \mathbf{k} and polarization vector \mathbf{u} for C_{55} and C_{66} .

trasond with the magnetic ions through the magnetoe-
lastic coupling acting on the exchange interactions, where
the exchange striction arises from an ultrasound modulation
of the exchange interactions [Eq. (2)] [13,14,22].
Moreover, the Curie-type softening in $C_r(T)$ is explained
by assuming the coupling of ultrasound to the structural
unit cells via the exchange striction mechanism, and the
presence of exchange-striction-sensitive inter-unit-cell in-
teractions. For the elastic modulus $C_r(T) = C_r^{(0)}(T) +$
 $\delta C_r^{sJT}(T)$ of the prototypical spin-JT system ACr_2O_4 ,
the contribution of the spin-JT component $\delta C_r^{sJT}(T)$ is
so large that the background component $C_r^{(0)}(T)$ can be
assumed to be T independent: $C_r^{(0)}(T) \simeq C_r^{(0)}(0)$ with
 $C_r^{(0)}(0)$ the background component at $T = 0$ K [14]. In
this case, the mean-field expression of $C_r(T)$ is written
as

$$C_r(T) = C_r^{(0)}(0) \frac{T - T_c}{T - \theta}. \quad (3)$$

Here, θ is the inter-unit-cell interaction, and $T_c = \theta +$
 $NG^2/C_r^{(0)}(0)$ is the second-order critical temperature for
elastic softening $C_r \rightarrow 0$ with N the number density of
the structural unit cell and G the constant of coupling of
the structural order parameter to the strain. θ is positive
(negative) when the interaction is ferrodistorative (antifer-

rodistorative).

For the spin-JT-active elastic modulus $C_r(T) =$
 $C_r^{(0)}(T) + \delta C_r^{sJT}(T)$ of CoTi_2O_5 , the contributions of
 $C_r^{(0)}(T)$ and $\delta C_r^{sJT}(T)$ are comparable, and we should
thus consider the T -dependent background $C_r^{(0)}(T)$. In
this case, Eq. (3) is rewritten as

$$C_r(T) = C_r^{(0)}(T) - \frac{NG^2}{T - \theta}, \quad (4)$$

where $\delta C_r^{sJT}(T) = -\frac{NG^2}{T - \theta}$. We now analyze the exper-
imental $C_{55}(T)$ and $C_{66}(T)$ of CoTi_2O_5 using Eq. (4)
with $N = 2.75 \times 10^{27} \text{ m}^{-3}$ [8]. For the T -dependent back-
ground $C_r^{(0)}(T)$, we adopt an empirical equation of the so-
called Varshni equation $C_r^{(0)}(T) = C_r^{(0)}(0) - A/(e^{B/T} - 1)$
with fitting parameters $C_r^{(0)}(0)$, A , and B [33]. In Fig.

TABLE II: Values of the fitting parameters in Eq. (4) for the
experimental $C_{55}(T)$ and $C_{66}(T)$ of CoTi_2O_5 [from the solid
curves in Fig. 4(c) and (d)].

	G (K)	θ (K)	$C_r^{(0)}(0)$ (GPa)	A (GPa)	B (K)
C_{55}	4630	-195	84.2	0.194	18.5
C_{66}	5810	-392	73.8	0.078	10.9

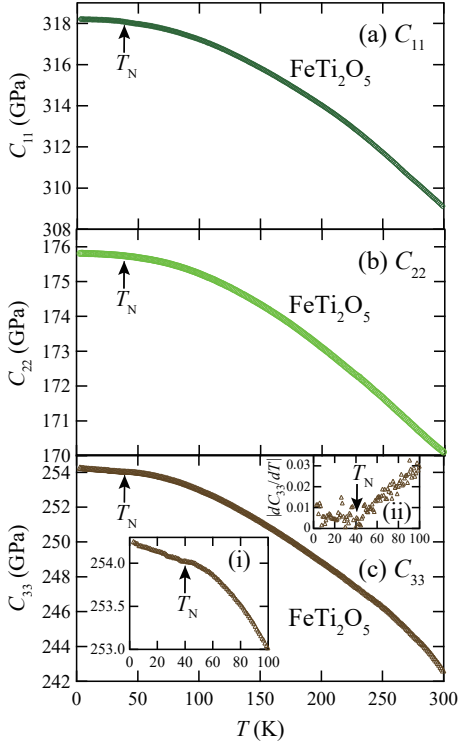


FIG. 5: (Color online) (a)–(c) Compressive elastic moduli of FeTi_2O_5 as functions of T : (a) $C_{11}(T)$, (b) $C_{22}(T)$, and (c) $C_{33}(T)$. The insets (i) and (ii) in (c) respectively show expanded views of $C_{33}(T)$ and $|dC_{33}(T)/dT|$ below 100 K. The labeled arrows indicate $T_N \sim 40$ K of FeTi_2O_5 .

4(c) and (d), respectively, fittings of Eq. (4) to the experimental $C_{55}(T)$ and $C_{66}(T)$ of CoTi_2O_5 are depicted as solid curves, which follow the experimental data well. Values for the fitting parameters are listed in Table II. In Fig. 4(c) and (d), $C_{\Gamma}^{(0)}(T)$ and $\delta C_{\Gamma}^{sJT}(T)$ in the fittings are respectively depicted as dashed-dotted and dotted curves, indicating that, for $C_{55}(T)$ and $C_{66}(T)$, the hardening magnitude of $C_{\Gamma}^{(0)}(T)$ and the softening magnitude of $\delta C_{\Gamma}^{sJT}(T)$ are comparable. In Table II, the fitting value of G for $C_{66}(T)$ ($G = 5810$ K) is larger than that for $C_{55}(T)$ ($G = 4630$ K), indicating that the magnetoelectric coupling in C_{66} is stronger than that in C_{55} . The negative fitting values of θ for $C_{55}(T)$ ($\theta = -195$ K) and $C_{66}(T)$ ($\theta = -392$ K) in Table II indicate the dominance of antiferrodistortive inter-unit-cell interactions that affect $C_{66}(T)$ more strongly than $C_{55}(T)$.

For CoTi_2O_5 , the spin-JT component $\delta C_{\Gamma}^{sJT}(T)$ is expected to be present in not only the symmetry-lowering elastic modes of shear moduli [Fig. 4(b)] but also the symmetry-conserving elastic modes of compressive moduli [Fig. 4(a)]. Comparing the compressive $C_{11}(T)$, $C_{22}(T)$, and $C_{33}(T)$ in Fig. 4(a), the hardening magnitude is smallest in the b -axis $C_{22}(T)$, which suggests that the contribution of the spin-JT component $\delta C_{\Gamma}^{sJT}(T)$ in the b -axis $C_{22}(T)$ is larger than that in the a -axis (spin-

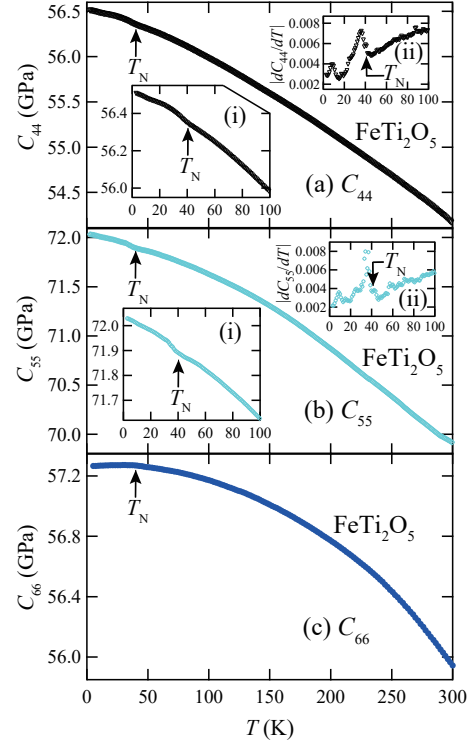


FIG. 6: (Color online) (a)–(c) Shear elastic moduli of FeTi_2O_5 as functions of T : (a) $C_{44}(T)$, (b) $C_{55}(T)$, and (c) $C_{66}(T)$. The insets (i) and (ii) in (a) and (b) respectively show the expanded views of $C_{55}(T)$, $|dC_{55}(T)/dT|$, $C_{66}(T)$, and $|dC_{66}(T)/dT|$ below 100 K. The labeled arrows indicate $T_N \sim 40$ K of FeTi_2O_5 .

chain-direction) $C_{11}(T)$. This reflects that, considering the exchange striction mechanism [Eq. (2)], the spin-lattice coupling along the interchain direction (b axis) is stronger than that along the spin-chain direction (a axis).

B. FeTi_2O_5

Figure 5(a)–(c) present the T dependence of the compressive elastic moduli $C_{11}(T)$, $C_{22}(T)$, and $C_{33}(T)$, respectively, in FeTi_2O_5 . $C_{11}(T)$ [Fig. 5(a)] and $C_{22}(T)$ [Fig. 5(b)] exhibit monotonic hardening upon cooling from 300 to 2 K, as is usually observed in solids [33]. Moreover, $C_{33}(T)$ [Fig. 5(c)] exhibits ordinary monotonic hardening upon cooling from 300 to $T_N \sim 40$ K and a small slope change of the hardening at $T_N \sim 40$ K. As mentioned in Sec. IIIA, for CoTi_2O_5 , the absence of an elastic anomaly at T_N in the spin-chain-direction (a -axis) compressive modulus $C_{11}(T)$ [Fig. 2(a)] rules out the possible spin-Peierls transition at T_N [30–32]. This is also the case for FeTi_2O_5 , where $C_{11}(T)$ exhibits no anomaly at T_N [Fig. 5(a)].

Figure 6(a)–(c) depict the T dependence of the shear elastic moduli $C_{44}(T)$, $C_{55}(T)$, and $C_{66}(T)$, respectively, in FeTi_2O_5 . $C_{66}(T)$ [Fig. 6(c)] exhibits monotonic hard-

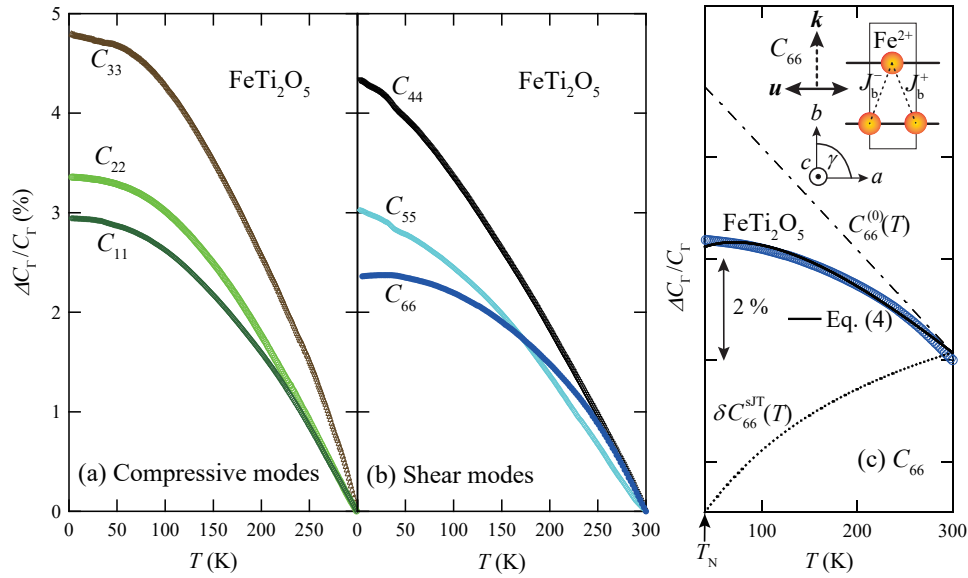


FIG. 7: (Color online) (a) and (b) Comparison of the relative shifts of the elastic moduli $C_\Gamma(T)$ of FeTi₂O₅: (a) compressive $C_{11}(T)$, $C_{22}(T)$, and $C_{33}(T)$ and (b) shear $C_{44}(T)$, $C_{55}(T)$, and $C_{66}(T)$. The experimental data in (a) and (b), respectively, are identical to those in Figs. 5 and 6. (c) Relative shift of $C_{66}(T)$ of FeTi₂O₅ at $T > T_N$ [circles, from (b)]. The solid curve in (c) is the fitting of Eq. (4) to the experimental $C_{66}(T)$. The dashed-dotted and dotted curves in (c) are respectively the background component $C_{66}^{(0)}(T)$ and spin-JT component $\delta C_{66}^{sJT}(T)$ in the fitting of Eq. (4). The inset in (c) illustrates the ab -plane projection of the unit cell shown in Fig. 1 along with the sound propagation vector \mathbf{k} and polarization vector \mathbf{u} for C_{66} .

ening upon cooling from 300 to 2 K. Moreover, $C_{44}(T)$ [Fig. 6(a)] and $C_{55}(T)$ [Fig. 6(b)] exhibit monotonic hardening upon cooling from 300 K to $T_N \sim 40$ K and a small slope change of the hardening at $T_N \sim 40$ K.

For FeTi₂O₅, Curie-type softening is not observed in any of the elastic moduli $C_\Gamma(T)$ [Figs. 5 and 6]. However, as mentioned in Sec. IIIA for CoTi₂O₅, it is expected for the low-symmetry spin-JT system that the elastic softness arising from the spin-JT effect is “hidden” in the elastic modulus $C_\Gamma(T)$, which exhibits hardening upon cooling. We should thus verify the presence of the “hidden” elastic softness also in $C_\Gamma(T)$ of FeTi₂O₅.

Similar to the discussion of CoTi₂O₅ in Sec. IIIA, we here compare the hardening magnitudes in $C_\Gamma(T)$ of FeTi₂O₅ [Figs. 5 and 6]. Figure 7 depicts the relative shifts of compressive $C_{11}(T)$, $C_{22}(T)$, and $C_{33}(T)$ of FeTi₂O₅ [Fig. 7(a), from Fig. 5] and shear $C_{44}(T)$, $C_{55}(T)$, and $C_{66}(T)$ of FeTi₂O₅ [Fig. 7(b), from Fig. 6]. Among the elastic moduli of FeTi₂O₅ in Fig. 7, $C_{66}(T)$ [Fig. 7(b)] exhibits the smallest hardening magnitude, which is similar to that for CoTi₂O₅ [Fig. 4]. Thus, for FeTi₂O₅, the symmetry-lowering elastic mode $C_{66}(T)$ should be characterized as a spin-JT-active elastic mode, which suggests the occurrence of the ab -plane shear (γ -tilt) lattice distortion at T_N [Fig. 1(b)]. However, the hardening magnitude of $C_{66}(T)$ in FeTi₂O₅ [Fig. 7(b)] is larger than that in CoTi₂O₅ [Fig. 4(b)], indicating that the spin-lattice coupling in FeTi₂O₅ is weaker than that in CoTi₂O₅.

For CoTi₂O₅, as mentioned in Sec. IIIA in conjunction with Figs. 3(b) and 4(b), not only $C_{66}(T)$ but also $C_{55}(T)$ are spin-JT-active elastic modes, where $C_{55}(T)$ exhibits Curie-type softening [Fig. 3(b)]. For FeTi₂O₅, comparing $C_{55}(T)$ with $C_{66}(T)$ [Fig. 7(b)], the hardening magnitude of $C_{55}(T)$ is smaller at higher values of T in the range of $170 \text{ K} \lesssim T < 300 \text{ K}$ but larger at lower values of T in the range of $T \lesssim 170 \text{ K}$. This indicates that, at lower values of T in the range of $T \lesssim 170 \text{ K}$ in Fig. 7(b), the spin-lattice coupling suppresses the hardening magnitude of $C_{66}(T)$ more strongly than that of $C_{55}(T)$. Thus, in the present study for FeTi₂O₅, although $C_{66}(T)$ should be characterized as a spin-JT-active elastic mode, $C_{55}(T)$ cannot be conclusively characterized as a spin-JT-active elastic mode, which is different from the case for CoTi₂O₅ [Sec. IIIA]. However, we can at least conclude that the contribution of the spin-lattice coupling to $C_{55}(T)$ of FeTi₂O₅ is, if present, less than that of CoTi₂O₅.

We here analyze the experimental $C_{66}(T)$ of FeTi₂O₅ using Eq. (4) with $N = 2.71 \times 10^{27} \text{ m}^{-3}$ [9], as done for

TABLE III: Values of the fitting parameters in Eq. (4) for the experimental $C_{66}(T)$ of FeTi₂O₅ [from the solid curve in Fig. 7(c)].

	G (K)	θ (K)	$C_\Gamma^{(0)}(0)$ (GPa)	A (GPa)	B (K)
C_{66}	4550	-192	60.8	0.350	30.8

CoTi₂O₅ in Sec. IIIA. In Fig. 7(c), the fitting of Eq. (4) to the experimental $C_{66}(T)$ of FeTi₂O₅ is depicted as a solid curve, which follows the experimental data well. Values for the fitting parameters are listed in Table III. In Fig. 7(c), $C_{66}^{(0)}(T)$ and $\delta C_{66}^{sJT}(T)$ in the fitting of Eq. (4) are respectively depicted as dashed-dotted and dotted curves, indicating that, for $C_{66}(T)$, the hardening magnitude of $C_{66}^{(0)}(T)$ and the softening magnitude of $\delta C_{66}^{sJT}(T)$ are comparable. The fitting value of G for $C_{66}(T)$ of FeTi₂O₅ ($G = 4550$ K in Table III) is smaller than that of CoTi₂O₅ ($G = 5810$ K in Table II), indicating that the magnetoelastic coupling is weaker in FeTi₂O₅ than in CoTi₂O₅. The negative fitting value of θ for $C_{66}(T)$ of FeTi₂O₅ ($\theta = -192$ K in Table III) indicates the dominance of antiferrodistortive inter-unit-cell interactions. This value is less than the antiferrodistortive θ in $C_{66}(T)$ of CoTi₂O₅ ($\theta = -392$ K in Table II).

For FeTi₂O₅, the spin-JT component $\delta C_{\Gamma}^{sJT}(T)$ is expected to be present in not only the symmetry-lowering elastic modes of shear moduli [Fig. 7(b)] but also the symmetry-conserving elastic modes of compressive moduli [Fig. 7(a)]. Comparing the compressive $C_{11}(T)$, $C_{22}(T)$, and $C_{33}(T)$ in Fig. 7(a), the hardening magnitude is smallest in the a -axis $C_{11}(T)$, which suggests that the contribution of the spin-JT component $\delta C_{\Gamma}^{sJT}(T)$ in the a -axis (spin-chain-direction) $C_{11}(T)$ is largest. This reflects that, considering the exchange striction mechanism [Eq. (2)], the spin-lattice coupling along the spin-chain direction (a axis) is stronger than that along the interchain directions (b and c axes), although the hardening magnitude of the b -axis $C_{22}(T)$ comparable to that of the a -axis $C_{11}(T)$ suggests that the spin-lattice coupling along the b axis is comparable to that along the a axis.

C. Spin-lattice coupling in ATi₂O₅ ($A = \text{Co, Fe}$)

The results of the present study conclude that the spin-JT effect emerges in both CoTi₂O₅ and FeTi₂O₅, but the relevant spin-lattice coupling in CoTi₂O₅ is stronger than that in FeTi₂O₅. Considering that the spin-JT mechanism in CoTi₂O₅ and FeTi₂O₅ should release the frustration of the interchain exchange interactions [Fig. 1], it is expected that the spin-lattice coupling along the interchain direction in CoTi₂O₅ is stronger than that in

FeTi₂O₅.

We here see the anisotropy of the elasticity or bond nature of CoTi₂O₅ and FeTi₂O₅ by comparing their compressive moduli. Table IV displays the room-temperature experimental values of the orthorhombic compressive moduli C_{11} , C_{22} , and C_{33} in CoTi₂O₅ [from Fig. 2], FeTi₂O₅ [from Fig. 5], and the spin-Peierls compound CuGeO₃ [35], where the spin-chain-direction modulus is the a -axis C_{11} for CoTi₂O₅ and FeTi₂O₅ and the c -axis C_{33} for CuGeO₃. Comparing CoTi₂O₅ and FeTi₂O₅ in Table IV, we see that the elasticity of CoTi₂O₅ is more isotropic than that of FeTi₂O₅. This is compatible with the spin-lattice coupling in CoTi₂O₅ being more isotropic than that in FeTi₂O₅, where, as mentioned above, the spin-lattice coupling along the interchain direction in CoTi₂O₅ is stronger than that in FeTi₂O₅.

In Table IV, comparing ATi₂O₅ ($A = \text{Co, Fe}$) with the spin-Peierls compound CuGeO₃, it is evident that, while the spin-chain-direction moduli of ATi₂O₅ (C_{11}) and CuGeO₃ (C_{33}) have the comparable values of $C_{\Gamma} \sim 300$ GPa, the elasticity of ATi₂O₅ is more isotropic and three-dimensional (3D) than the highly-anisotropic 1D elasticity of CuGeO₃, although the elasticity of FeTi₂O₅ is less isotropic than that of CoTi₂O₅. This 3D bond nature of ATi₂O₅ is compatible with the spin-lattice coupling in ATi₂O₅ having an isotropic 3D character whereas that in CuGeO₃ having an anisotropic 1D character. It is thus suggested for ATi₂O₅ that, although the nature of exchange interactions is quasi-1D [10,12], the 3D spin-lattice coupling enables a spin-JT mechanism that releases the frustration of the interchain exchange interactions. The present study demonstrates that the spin-JT effect can emerge in a low-dimensional spin system that has 3D spin-lattice coupling.

IV. SUMMARY

Ultrasound velocity measurements of the orthorhombic pseudobrookites CoTi₂O₅ and FeTi₂O₅ revealed the unusual elastic softness of the symmetry-lowering elastic modes of shear elastic moduli above T_N , namely the ab -plane shear C_{66} and ac -plane shear C_{55} for CoTi₂O₅, and the ab -plane shear C_{66} for FeTi₂O₅. This elastic softness indicates the presence of spin-lattice-coupled fluctuations above T_N , which are driven by spin-lattice coupling along the interchain direction and should be a precursor to symmetry-lowering lattice distortion at T_N . It is thus concluded that CoTi₂O₅ and FeTi₂O₅ are unique spin-JT systems with low crystal symmetry, where the frustration is released by further lowering the crystal symmetry through spin-lattice coupling. Furthermore, the ultrasound velocity measurements revealed that the magnitude of the unusual elastic softness is larger in CoTi₂O₅ than in FeTi₂O₅, indicating that the spin-lattice coupling along the interchain direction is stronger in CoTi₂O₅ than in FeTi₂O₅. For CoTi₂O₅ and FeTi₂O₅, the results of the present study suggests that, although the nature

TABLE IV: Room-temperature experimental values of the orthorhombic compressive moduli C_{11} , C_{22} , and C_{33} in CoTi₂O₅ [from Fig. 2], FeTi₂O₅ [from Fig. 5], and the spin-Peierls compound CuGeO₃ [35]. The values of the spin-chain-direction compressive moduli in the respective compounds are underlined.

	CoTi ₂ O ₅	FeTi ₂ O ₅	CuGeO ₃
C_{11} (GPa)	<u>333</u>	<u>309</u>	64
C_{22} (GPa)	328	170	38
C_{33} (GPa)	319	243	<u>317</u>

of exchange interactions is quasi-1D, the spin-JT effect is driven by 3D spin-lattice coupling.

V. ACKNOWLEDGMENTS

This work was partly supported by a Grant-in-Aid for Scientific Research (C) (Grant No. 21K03476) from

MEXT of Japan. DP acknowledges the Engineering and Physical Sciences Research Council (EPSRC), UK grant number EP/R024278/1 and the Oxford-ShanghaiTech collaboration project for financial support.

-
- * Electronic address: watanabe.tadataka@nihon-u.ac.jp
- ¹ C. Lacroix, P. Mendels, and F. Mila, eds., *Introduction to Frustrated Magnetism: Materials, Experiments, Theory*, Vol. 164 (Springer, 2011).
 - ² Y. Yamashita and K. Ueda, Phys. Rev. Lett. **85**, 4960 (2000).
 - ³ O. Tchernyshyov, R. Moessner, and S. L. Sondhi, Phys. Rev. Lett. **88**, 067203 (2002).
 - ⁴ G. A. Gehring and K. A. Gehring, Rep. Prog. Phys. **38**, 1 (1975).
 - ⁵ S. -H. Lee, C. Broholm, T. H. Kim, W. Ratcliff II, and S. W. Cheong, Phys. Rev. Lett. **84**, 3718 (2000).
 - ⁶ L. Ortega-San-Martín, A. J. Williams, C. D. Gordon, S. Klemme, and J. P. Attfield, J. Phys.: Condens. Matter **20**, 104238 (2008).
 - ⁷ J. -H. Chung, M. Matsuda, S. -H. Lee, K. Kakurai, H. Ueda, T. J. Sato, H. Takagi, K. -P. Hong, and S. Park, Phys. Rev. Lett. **95**, 247204 (2005).
 - ⁸ Franziska K. K. Kirschner, Roger D. Johnson, Franz Lang, Dmitry D. Khalyavin, Pascal Manuel, Tom Lancaster, Dharmalingam Prabhakaran, and Stephen J. Blundell, Phys. Rev. B **99**, 064403 (2019).
 - ⁹ Franz Lang, Lydia Jowitt, Dharmalingam Prabhakaran, Roger D. Johnson, and Stephen J. Blundell, Phys. Rev. B **100**, 094401 (2019).
 - ¹⁰ Hao-Hang Xu, Qing-Yuan Liu, Chao Xin, Qin-Xin Shen, Jun Luo, Rui Zhou, Jin-Guang Cheng, Jian Liu, Ling-Ling Tao, Zhi-Guo Liu, Ming-Xue Huo, Xian-Jie Wang, and Yu Sui, Chin. Phys. B **33**, 037505 (2024).
 - ¹¹ Dylan Behr, Leonid S. Taran, Daniel G. Porter, Alessandro Bombardi, Dharmalingam Prabhakaran, Sergey V. Streltsov, and Roger D. Johnson, Phys. Rev. B (to be published).
 - ¹² Hao-Hang Xu, Jian Liu, L. L. Tao, Xian-Jie Wang, Sergey V. Streltsov, and Yu Sui, Phys. Rev. B **109**, 184430 (2024).
 - ¹³ B. Lüthi, *Physical Acoustics in the Solid State* (Springer, 2005).
 - ¹⁴ T. Watanabe, S. Ishikawa, H. Suzuki, Y. Kousaka, and K. Tomiyasu, Phys. Rev. B **86**, 144413 (2012).
 - ¹⁵ Subhro Bhattacharjee, S. Zherlitsyn, O. Chiatti, A. Sytcheva, J. Wosnitza, R. Moessner, M. E. Zhitomirsky, P. Lemmens, V. Tsurkan, and A. Loidl, Phys. Rev. B **83**, 184421 (2011).
 - ¹⁶ T. Watanabe, S. Hara, and S. Ikeda, Phys. Rev. B **78**, 094420 (2008).
 - ¹⁷ T. Watanabe, S. Hara, S. Ikeda, and K. Tomiyasu, Phys. Rev. B **84**, 020409(R) (2011).
 - ¹⁸ Y. Nii, N. Abe, and T. Arima, Phys. Rev. B **87**, 085111 (2013).
 - ¹⁹ T. Watanabe, T. Ishikawa, S. Hara, A. T. M. N. Islam, E. M. Wheeler, and B. Lake, Phys. Rev. B **90**, 100407(R) (2014).
 - ²⁰ T. Watanabe, S. Takita, K. Tomiyasu, and K. Kamazawa, Phys. Rev. B **92**, 174420 (2015).
 - ²¹ T. Watanabe, S. Yamada, R. Koborinai, and T. Katsufuji, Phys. Rev. B **96**, 014422 (2017).
 - ²² T. Watanabe, S. Kobayashi, Y. Hara, J. Xu, B. Lake, J.-Q. Yan, A. Niazi, and D. C. Johnston, Phys. Rev. B **98**, 094427 (2018).
 - ²³ T. Watanabe, H. Kato, Y. Hara, J. W. Krizan, and R. J. Cava, Phys. Rev. B **101**, 214425 (2020).
 - ²⁴ T. Watanabe, R. Okada, and K. Tomiyasu, Phys. Rev. B **106**, 144432 (2022).
 - ²⁵ Y. Kino, B. Lüthi, and M. E. Mullen, J. Phys. Soc. Jpn. **33**, 687 (1972); Solid State Commun. **12**, 275 (1973).
 - ²⁶ M. Kataoka and J. Kanamori, J. Phys. Soc. Jpn. **32**, 113 (1972).
 - ²⁷ H. Hazama, T. Goto, Y. Nemoto, Y. Tomioka, A. Asamitsu, and Y. Tokura, Phys. Rev. B **62**, 15012 (2000).
 - ²⁸ B. Kindler, D. Finsterbusch, R. Graf, F. Ritter, W. Assmus, and B. Lüthi, Phys. Rev. B **50**, 704 (1994).
 - ²⁹ B. J. Ramshaw, A. Shekhter, R. D. McDonald, J. B. Betts, J. N. Mitchell, P. H. Tobash, C. H. Mielke, E. D. Bauer, and A. Migliori, PNAS **112**, 3285 (2015).
 - ³⁰ M. Saint-Paul, G. Reményi, N. Hegmann, P. Monceau, G. Dhalenne, and A. Revcolevschi, Phys. Rev. B **52**, 15298 (1995).
 - ³¹ M. Poirier, M. Castonguay, A. Revcolevschi, and G. Dhalenne, Phys. Rev. B **52**, 16058 (1995).
 - ³² H. Schwenk, S. Zherlitsyn, B. Lüthi, E. Morre, and C. Geibel, Phys. Rev. B **60**, 9194 (1999).
 - ³³ Y. P. Varshni, Phys. Rev. B **2**, 3952 (1970).
 - ³⁴ H. Stern, J. Phys. Chem. Solids **26**, 153 (1965).
 - ³⁵ C. Ecolivet, M. Saint-Paul, G. Dhalenne, and A. Revcolevschi, J. Phys.: Condens. Matter **11**, 4157 (1999).